International Journal of Heat and Mass Transfer 52 (2009) 2721–2732

Contents lists available at ScienceDirect

International Journal of Heat and Mass Transfer

journal homepage: www.elsevier.com/locate/ijhmt

Topology optimization for thermal conductors considering design-dependent effects, including heat conduction and convection

A. Iga *, S. Nishiwaki, K. Izui, M. Yoshimura

Department of Aeronautics and Astronautics, Kyoto University, Yoshida Honmachi, Sakyo-ku, Kyoto City 606-8501, Japan

ARTICLE INFO

Article history:
Received 10 May 2008
Received in revised form 19 November 2008
Available online 14 February 2009

Keywords:
Topology optimization
Heat conduction
Heat convection
Structural analysis
Homogenization theory

ABSTRACT

In structural designs considering thermal loading, in addition to heat conduction within the structure, the heat convection upon the structure's surface can significantly influence optimal design configurations. In this paper, we focus on the influence of design-dependent effects upon heat convection and internal heat generation for optimal designs developed using a topology optimization scheme. The method for extracting the structural boundaries for heat convection loads is constructed using a Hat function, and heat convection shape dependencies are taken into account in the heat transfer coefficient using a surrogate model. Several numerical examples are presented to confirm the usefulness of the proposed method.

1. Introduction

For structural designs considering thermal loading, maximization of temperature diffusivity in the structure is one of the most important factors in reducing operating temperature and maintaining product durability, in addition to the usual maximization of stiffness that solutions to optimal design problems aim to achieve. One way to obtain design solutions incorporating maximization of temperature diffusivity and stiffness is to apply a structural optimization method.

Topology optimization [1] has been primarily applied to structural problems and it is considered the most flexible structural optimization method because it allows changes in topology as well as shape. Most topology optimization studies focus on structural problems such as stiffness maximization [2] and eigenfrequency maximization [3].

Thermal problems have mainly been discussed in the context of basic topology optimization theory using a homogenization method [4–7], due to their relatively simple constitutive equations. Topology optimization methods based on the Solid Isotropic Material with Penalization (SIMP) method [8] have been proposed and applied to thermal problems [9]. Li et al. [10,11] extended the evolutionary structural optimization (ESO) method [12] to fulfill shape and topology design in steady-state heat conduction problems. Gersborg-Hansen and Bendsøe [13] compared the optimization results of two heat conduction problems that were solved by the finite element method and finite volume method, respectively. Li et al. implemented a method for dealing with transient heat conduction for topology designs [14].Sigmund et al. investigated the effects that thermal considerations have on material layout designs and introduced concepts for dealing with heat transfer and electrical conduction in the inherently metaphysical topology design problems for micro-electromechanical (MEMS) systems [15]. On the other hand, Zhuang et al. [16] developed level set-based topology optimization methods for thermal problems, where the optimization process was updated with so-called topological derivatives, using the finite difference method.

In these previous conventional topology optimization methods, due to the inability to precisely define structural boundaries in the fixed design domain, boundary conditions such as heat transfer boundary conditions, which should be set on the structural boundaries, could not be defined, and therefore, the design-dependent effects of the heat transfer coefficients could not be considered. Similar boundary condition problems for considering design-dependent effects such as pressure loads, self-weight, and centrifugal loads are also observed in the structural problems.

To overcome the issue of setting boundary conditions, Chen and Kikuchi [17] proposed a way for dealing with design-dependent effects for structural problems where pressure loads were set on structural boundaries by using the fictitious fluid elements in the void region of the fixed design domain, without setting pressure loads on structural boundaries directly, so that design-dependent effects concerning pressure loads can be treated during the optimization process. Bourdin and Chamblle [18] also proposed design-dependent loads in topology optimization where a structure was represented as a subset of reference domain, and the complement of the subset was made of two other phases, the void and a

* Corresponding author. Tel.: +81 749 52 8406; fax: +81 749 52 6346.
E-mail address: atsuro_iga@yanmar.co.jp (A. Iga).

0017-9310/$ - see front matter © 2009 Elsevier Ltd. All rights reserved.
doi:10.1016/j.ijheatmasstransfer.2008.12.013

Nomenclature

A	area
a_j	interpolation expansion coefficient
b	internal heat generation
Bi	Biot number
b^h	descretized internal heat generation
D	fixed design domain
F	total potential energy
g	volume
g_j	Radial Basis Function
h	heat transfer coefficient
h^h	descretized heat transfer coefficient
h_0	nodal heat transfer coefficient
$\boldsymbol{h}$	vector of heat transfer coefficient
H	Hat function
$\boldsymbol{H}$	heat transfer vector
K	coefficient of heat transmission
$\boldsymbol{K}$	thermal conduction matrix
$\boldsymbol{K}_h$	heat transfer matrix
l	length
n	the total number of nodes
N_i^r	shape functions
Nu	Nusselt number
m	position of sampling points
$\mathbf{N}^r$,$\mathbf{M}^r$	vector of shape functions
P	fin period
Pr	Prandtl number
$\boldsymbol{q}$	heat flux vector
q_{react}	reaction of applied heat flux
$\mathbf{Q}$	internal heat generation vector
r	design variable
r^h	descretized design variable
$\boldsymbol{R}$	vector of nodal design variables
Re	Reynolds number
R_i	design variables on nodes
R_{upp}	upper bound of design variables
S	area
T	temperature
$\boldsymbol{T}$	temperature vector
$\tilde{T}$	virtual temperature
T_{amb}	ambient temperature
$\boldsymbol{x}$	position in the fixed design domain
$\mathbf{y}$	position in the micro structure
Y	unit cell area

Greek symbols

Γ_q	heat flux boundary
Γ_h	heat convection boundary
Γ_T	temperature boundary
ε	size of bandwidth in Hat function
$\boldsymbol{\kappa}$	thermal conduction tensor
$\boldsymbol{\kappa}^H$	homogenized thermal conduction tensor
λ	thermal conductivity
ρ	node density
ρ_e	element density
$\boldsymbol{\xi}$	characteristic temperature filed
χ_Ω	characteristic function
Ω_d	original design domain
Ω_s	upper limit of volume constrain

fictitious liquid that exerted a pressure load on its interface with the solid structure. For heat conduction problems, Gao et al [19] investigated and compared design-dependent effects using ESO, but did not consider heat convection problems. Yoo and Kim proposed the Element Connectivity Parameterization (ECP) method [20] to consider design-dependent effects for thermal problems with heat transfer boundaries, but this leads to theoretical inconsistencies with continuum mechanics. Ryu and Kim [21], and Bruns [22] proposed a way to extract the structural boundaries of thermal problems, but did not consider shape dependencies with respect to heat transfer coefficients.

To solve the above issues concerning the setting of boundary conditions for thermal problems, we propose a new topology optimization method for thermal problems having generic thermal boundary conditions such as heat flux, heat convection and internal heat generation that includes design-dependent effects. First, the concept of basic topology optimization theory based on the homogenization method is briefly discussed. The objective function of the optimization problem is then formulated using the concept of total potential energy, so that the optimization problems can be treated as objective function maximization problems for both Neumann and Dirichlet type boundary conditions. Next, a newly developed method for dealing with design-dependent effects that pertain to heat convection and internal heat generation loads is explained. In this method, the heat transfer boundaries between material and void regions that emerge in the fixed design domain are extracted using a Hat function so that the heat transfer coefficients can be set on these boundaries. The shape dependencies of the heat transfer coefficients in the formulation are also discussed, and a method to represent such shape dependencies is developed via a surrogate model using the Radial Basis Function. An optimization algorithm is constructed using the Finite Element Method and Sequential Linear Programming. Finally, several numerical examples that address thermal problems are provided to confirm the usefulness of the proposed method.

2. Formulation of topology optimization method for thermal problems

Here we briefly discuss a topology optimization method for thermal problems with generic thermal boundary conditions such as heat flux, internal heat generation and heat convection loads that include design-dependent effects, based on the homogenization method. In this method, continuous approximation of material distribution is assumed for implementation.

2.1. Basic topology optimization theory based on the homogenization method

In this research, we introduce the homogeneous design method (HDM) theory in which a continuous material distribution is assumed, using a continuous interpolation function at each node.

The key idea of the topology optimization method is the introduction of a fixed design domain D that includes the original design domain Ω_d and the following characteristic function.

$$\chi_\Omega](\boldsymbol{x}) = \begin{cases} 1 & \text{if } \boldsymbol{x} \in \Omega_d \\ 0 & \text{if } \boldsymbol{x} \in D \setminus \Omega_d \end{cases} \tag{1}$$

where $\boldsymbol{x}$ denotes a position in the extended design domain D. Using this characteristic function χ_Ω and the extended design domain D, the original structural problem is replaced by a material distribution problem incorporating an thermal conduction tensor $\chi_\Omega{}^{\boldsymbol{\kappa}}$, in the extended design domain D, where $\boldsymbol{\kappa}$ is the thermal conduction

tensor in the original design domain Ω_d. Since this type of characteristic function is highly discontinuous, namely, lies in $L^\infty(D)$, some regularization or smoothing technique must be introduced for the numerical treatment. A homogenization method is used to carry out the relaxation of the design domain by introducing microstructures to represent the composite material status. In two scale modeling, which is based on the asymptotic homogenization method, microstructures are continuously distributed almost everywhere in the extended design domain D, and this status must hold even after the finite element discretization. In this work, the HDM method is applied to temperature diffusivity optimization problems. In the conventional HDM [4–7] and also SIMP [8,9] methods, however, the design variables are approximated by piecewise constants in the finite element implementation, and a discontinuous material distribution over the elements can be the cause of numerical instability such as checkerboards. To overcome such problems, several methods have been proposed, such as the use of filtering schemes [23,24] and the perimeter control method [25]. Although the filtering schemes and the perimeter control method are now popular means for avoiding these numerical problems, these methods crucially depend on the use of artificial parameters for which there are no rational guideline to follow when determining the appropriate parameter values required for additional constraints. To overcome the above problems and maintain procedural consistency, Matsui and Terada [26] proposed a topology optimization method with assumed continuous approximation of material distribution, in which the design variable $r(\boldsymbol{x})$ is expressed as

$$r(\boldsymbol{x}) \approx r^h(\boldsymbol{x}) = \boldsymbol{N}^r(\boldsymbol{x})\boldsymbol{R} = \sum_{i=1}^{n} N_i^r R_i \tag{2}$$

where r^h stands for the discretized quantity using the finite element method (FEM), $\mathbf{N}^r$ is a vector whose components are $N_i^r (i = 1,\cdots,n)$, $\mathbf{R}$ is a vector of nodal design variables whose components are R_i $(i = 1,\cdots, n)$ and n is the total number of nodes in the fixed design domain D, which is also the same as the number of design variables in this formulation. Using the above formulation, the design variables can maintain the C^0-continuity over the domain. In this research, the above formulation is employed for the approximation of design variables. A bilinear interpolation function is used as $N_i^r(\boldsymbol{x})$ in the case of four-node quadrilateral elements, and because it preserves the C^0-continuity. Note that since the discrete material densities of the design variables are computed at each node in this formulation. Also note that a similar formulation based on the SIMP method was presented by Rahmatalla and Swan [27].

Fig. 1 shows the microstructure used for the relaxation of the design domain in the two-dimensional problem. As shown, the microstructure is square and the design variable is a geometrical parameter r that must respectively be 1 or 0 for void or material to be present.

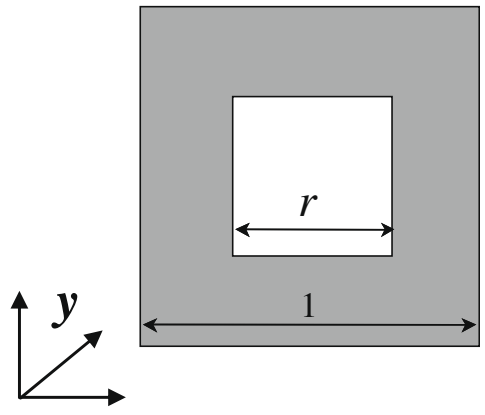

Fig. 1. Microstructure used for the relaxation of design domain.

$$0 \leqslant r \leqslant 1 \tag{3}$$

Note that this microstructure has an isotropic response and is sufficient for our design problems.

As we explained above, the homogenization method is introduced to compute the physical properties in the global and local sense using multi-scale modeling and asymptotic expansion. Using this method, the homogenized or average physical properties in the global or macroscopic sense are obtained by the homogenization procedure using a microstructure defined in the local or microscopic coordinate. See details in [28,29].

Here we briefly explain how the homogenized thermal conduction tensor $\boldsymbol{\kappa}^H$ is obtained. First, a characteristic temperature ξ is obtained by solving the following linearized equilibrium equation in the microscopic coordinate system:

$$\int_Y \boldsymbol{\kappa}(\boldsymbol{y})\nabla_y \bar{T}\nabla_y \xi(\boldsymbol{y})dy = \int_Y \boldsymbol{\kappa}(\boldsymbol{y})\nabla_y \bar{T}dy \quad \forall \bar{T} \in V_y \tag{4}$$

where V_y is the admissible space defined in a unit cell Y such that

$$V_y = \{\bar{T}(\boldsymbol{y}) | \bar{T}_i \in H^1(Y), \bar{T}(\boldsymbol{y}) : Y - \text{periodic on } Y\} \tag{5}$$

where $H^1(Y)$ indicates a Sobolev space.

Using the above characteristic temperature ξ, the homogenized thermal conduction tensor $\boldsymbol{\kappa}^H$ with respect to design variable defined in the local or microscopic coordinate system is obtained by

$$\boldsymbol{\kappa}^H(\boldsymbol{x}) = \frac{1}{|Y|}\int_Y \boldsymbol{\kappa}(\boldsymbol{y})(\boldsymbol{I} - \nabla_y \xi(\boldsymbol{y}))dy \tag{6}$$

where $\boldsymbol{\kappa}(\mathbf{y})$ and ∇_y respectively indicate the thermal conduction tensor in the microscopic sense and the differential operator with respect to the y coordinate that indicates a local coordinate defined in the microstructure as shown in Fig. 2, and $|Y|$ indicates the area of the unit cell. Note that the macroscopic variables are defined almost everywhere in the macro-structure and obtained as the volume average of the microscopic physical properties, which are evaluated by solving microscopic problems. That is, a microscopic problem is defined at each material point in macro-scale. Thus the relationship between a unit cell design variable and the homogenized thermal conduction tensor is established.

2.2. Formulation of thermal problems

In this section, we formulate the generic temperature diffusivity optimization problems for linear thermal conductors.

Here we consider a two-dimensional steady-state heat conduction problem. Suppose that an arbitrary linear thermal conductor occupies domain Ω_d with boundary Γ and thermal conduction tensor is $\boldsymbol{\kappa}^H(\boldsymbol{x})$, derived from Eq. (6). Then the temperature field T within the domain is governed by the following equation.

$$\nabla \cdot (\boldsymbol{\kappa}^H \nabla T) + b = 0 \tag{7}$$

where b indicates the internal heat generation in Ω_d. With $\tilde{T}$ representing the virtual temperature field, the equilibrium equation of a

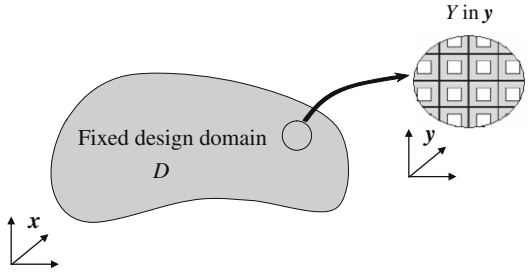

Fig. 2. Two-scale modeling for the periodic porous body.

linear thermal conductor can then be rewritten as the following weak form, through the principle of virtual temperature [30]:

$$\int_{\Omega_d} \nabla\tilde{T}\boldsymbol{\kappa}^H\nabla T d\Omega - \int_{\Gamma} \tilde{T}\boldsymbol{\kappa}^H \frac{\partial T}{\partial n} d\Gamma + \int_{\Omega_d} b\tilde{T} d\Omega = 0 \tag{8}$$

We consider the boundary conditions for a linear thermal conductor whose temperature field is denoted as T. We also impose a temperature $T = 0$ °C on Γ_T, $T = c(\boldsymbol{x}) \neq 0$ °C on Γ_c, heat flux q on Γ_q and a heat convection load consisting of heat transfer coefficients h and ambient temperature $T = T_{\mathrm{amb}}$ on Γ_h. The equilibrium equation of a linear thermal conductor is then formulated as follows,

$$a(T,\tilde{T}) + L_c(\tilde{T}) = L(\tilde{T}) \quad \forall\tilde{T} \in V \tag{9}$$

where $a(T,\tilde{T})$ is a bilinear form such that

$$a(T,\tilde{T}) = \int_{\Omega_d} \nabla\tilde{T}\boldsymbol{\kappa}^H\nabla T d\Omega + \int_{\Gamma_h} \tilde{T}hT d\Gamma \tag{10}$$

and

$$L_c(\tilde{T}) = \int_{\Gamma_c} \nabla\tilde{T}\boldsymbol{\kappa}^H\nabla c d\Gamma = \int_{\Gamma_c} q_{react}(\tilde{T}) c d\Gamma \tag{11}$$

$$L(\tilde{T}) = \int_{\Gamma_q} q\tilde{T} d\Gamma + \int_{\Omega_d} b\tilde{T} d\Omega + \int_{\Gamma_h} hT_{amb}\tilde{T} d\Gamma \tag{12}$$

q_{react} indicates the reaction of the heat flux which acts on Γ_c, and V is a subset of a Sobolev space in which admissible temperatures are defined as follows:

$$V = \{\tilde{T}(\boldsymbol{x}) | \tilde{T}_i \in H^1(\Omega_d), \text{ and } \tilde{T} = 0 \text{ on } \Gamma_T\tilde{T} = c \text{ on } \Gamma_c\} \tag{13}$$

Next, we formulate the objective function that will be used when formulating the thermal conductor design problems. Here we define the mean temperature, which corresponds to the mean compliance in the structural problems.

$$T_{mean} = \int_{\Gamma_q} qT d\Gamma + \int_{\Omega_d} bT d\Omega + \int_{\Gamma_h} h(T_{amb} - T) T d\Gamma + \int_{\Gamma_c} q_{react}(T) c d\Gamma \tag{14}$$

For the case where only the heat flux boundary condition is considered, the mean temperature is expressed as;

$$T_{mean} = \int_{\Gamma_q} qT d\Gamma \tag{15}$$

Then, temperature at Γ_q is minimized by minimizing the mean temperature, and consequently, the temperature diffusion is maximized. On the other hand, for the case where a fixed temperature on boundary Γ_c is considered, mean temperature is written as;

$$T_{mean} = \int_{\Gamma_c} q_{react}(T) c d\Gamma = a(T,T) \tag{16}$$

In this case, the reaction heat flux q_{react} is maximized for given temperature at Γ_c by maximizing the mean temperature, and as a result, temperature diffusion is maximized. Thus, when the mean temperature is used as an objective function, it is difficult to determine whether the mean temperature should be minimized or maximized since this determination crucially depends on the boundary setting. To overcome this problem, we formulate the total potential energy as the objective function as follows, based on the concept of the total potential energy used in the usual stiffness maximization problems.

$$F(T) = \frac{1}{2}a(T,T) - L(T) \tag{17}$$

Using the above formulation, the optimization problems can be treated as an objective function maximization problem for both Neumann (i.e., heat flux boundary) and Dirichlet (i.e., temperature boundary) type boundary conditions, so we can formulate the optimization problem for maximization of temperature diffusivity under the volume constraint of the materials as

$$\textit{Maximize } F(T) \tag{18}$$

subject to

$$g = \int (1 - r^2) d\Omega \leqslant \Omega_s \quad \text{and Eqs. (3)} \quad \text{and} \quad (9) \tag{19}$$

where Ω_s indicates the upper limit of the volume constraint. Thus, we can minimize the temperature in the designed thermal conductors by maximizing the total potential energy, which maximizes temperature diffusivity in the thermal conductor.

2.3. Formulation of design-dependent internal heat generation loads

Since the amount of internal heat generation usually depends on the material density, the quantity of internal heat generation changes as the material density changes. Here, we assume that that the internal heat generation loads are proportional to the material density. Then, the design-dependent internal heat generation loads are formulated using the characteristic function χ_Ω in the domain as follows:

$$\int_{\Omega_d} b\tilde{T} \mathrm{d}\Omega = \int_D \chi_\Omega b\tilde{T} \mathrm{d}\Omega \tag{20}$$

where b is the internal heat generation at point $\boldsymbol{x}$ in the fixed design domain D.

By applying the relaxation scheme for the design domain, the internal heat generation b is expressed as

$$b(\boldsymbol{x}) \approx b^h(\boldsymbol{x}) = b_0(1 - r^{h2}) \tag{21}$$

where b^h indicates the discretized internal heat generation and b_0 indicates the internal heat generation value per unit volume. In the case of solid areas, a density of 1 is implied.

Using the above equation, the internal heat generation loads can change in response to shape changes because the internal heat generation loads are expressed as a function of design variables $r(\boldsymbol{x})$.

2.4. Formulation of design-dependent heat convection loads

In conventional topology optimization methods, due to the inability to precisely set structural boundaries in the fixed design domain, boundary conditions such as heat transfer boundary conditions, which should be set on the structural boundaries, cannot be precisely represented. To overcome this issue, we construct a new method for dealing with heat transfer boundaries between material and void regions that emerge in the fixed design domain.

Topology optimization yields optimal configurations as a material density distribution, and areas of intermediate density (e.g., gray scale areas) often emerge during the optimization procedure. Such areas can be considered as boundaries between solid and void regions, and to extract these structural boundaries, we introduce the following Hat function (a smeared-out Hat function) as a function of the element density ρ_e calculated using the nodal densities in each element.

$$H(\rho_e) = \begin{cases} 0 & \rho_e < \rho_{lower} - \varepsilon \\ \frac{1}{2} + \frac{(\rho_e - \rho_{lower})}{2\varepsilon} + \frac{1}{2\pi}\sin\left\{\frac{\pi(\rho_e - \rho_{lower})}{\varepsilon}\right\} & \rho_{lower} - \varepsilon < \rho_e < \rho_{lower} + \varepsilon \\ 1 & \rho_{lower} + \varepsilon < \rho_e < \rho_{upper} - \varepsilon \\ \frac{1}{2} - \frac{(\rho_e - \rho_{upper})}{2\varepsilon} - \frac{1}{2\pi}\sin\left\{\frac{\pi(\rho_e - \rho_{upper})}{\varepsilon}\right\} & \rho_{upper} - \varepsilon < \rho_e < \rho_{upper} + \varepsilon \\ 0 & \rho_{upper} + \varepsilon < \rho_e \end{cases} \tag{22}$$

where ρ_{lower} and ρ_{upper} are respectively the lower and upper limit values for the extraction of boundaries for setting the heat convection loads, and $\rho_e < \rho_{lower}$ for voids, $\rho_{upper} < \rho_e$ for material, and $\rho_{lower} < \rho_e < \rho_{upper}$ for structural boundaries, where ε in the above equation determines the size of the bandwidth of numerical smearing in the Hat function, to avoid numerical singularities.

Next, we set the heat transfer coefficients on all nodes in the finite element model and arrange them uniformly over the entire design domain using the shape function, as shown in Fig. 3(a). Then, using the smeared-out Hat function, heat transfer coefficients can be set on the structural boundaries extracted by Eq. (22), as shown in Fig. 3(b). The heat transfer coefficients are approximated as:

$$h(\boldsymbol{x}) \approx h^h(\boldsymbol{x}) = H(\rho_e)\boldsymbol{M}^r(\boldsymbol{x})\boldsymbol{h} = H(\rho_e)h_0\sum_{i=1}^{n} M_i^r(\boldsymbol{x}) \tag{23}$$

where h^h and h_0 stand for the discretized heat transfer coefficient and the nodal heat transfer coefficient, respectively. $\boldsymbol{M}^r$ is a vector whose components are M_i^r ($i = 1,\cdots,n$), $\boldsymbol{h}$ is a vector of the nodal heat transfer coefficients, all of whose components are h_0. Here a bilinear interpolation function is also used as $M_i^r(\boldsymbol{x})$ in the case of four-node quadrilateral elements. Thus, the heat transfer coefficients can be set on the structural boundaries while maintaining the C^0-continuity on the structural boundaries.

2.5. Shape dependencies concerning heat transfer coefficients

Formulations of the heat transfer coefficient have been derived experimentally and theoretically for various cases. For example, Eqs. (24) and (25) show the Dittus and Boelter formulation for heat transfer in a pipe containing a turbulent fluid [31]. This formulation is valid for the range of $10^4 < Re < 10^5$ and $1 < Pr < 10$.

$$Nu = 0.023Re^{0.8}Pr^{0.4} \quad \text{and} \tag{24}$$

$$h = \frac{\lambda_{fluid}}{d}Nu \tag{25}$$

where Nu, Re, Pr and d indicate the Nusselt, Reynolds and Prandtl numbers, and diameter of the pipe, respectively. As shown in these equations, heat transfer coefficients are strongly correlated with fluid velocity, so it is important that the influence of fluid velocity be considered when setting them. In addition to structural changes, heat transfer coefficients must also be considered changeable in response to structural changes, due to shape dependencies. In previous work [20–22], only the structural boundary information is extracted, and the shape dependencies of the heat transfer coefficients were not considered, due to the complexity of heat transfer phenomena that are strongly correlated with fluid–structure interactions. One possible way to examine such dependencies would be to apply coupled numerical fluid-thermal analysis, but this is computationally intensive, and at early design stages, simplified models enable more rapid development of basically sound designs, which is the desired goal. We therefore propose a new scheme for updating the heat transfer coefficients in response to structural changes during the optimization, using a surrogate model that considers the relationships between shape and heat transfer coefficients, as described below.

First, to quantify the relationships of shape and heat transfer coefficients, we conduct numerical fluid analysis for models having different arrangements of fins. In our research, three models are constructed, CASE (1)–(3) shown in Fig. 4(1), all of which have the same fin height, but incorporate different periodic spacing. Fig. 4(2) shows the numerical fluid simulation model. Fins which are defined in Fig. 4(1) are positioned at the bottom middle of simulation model. We assume that the fluid temperature is 0 °C with a 1 m/s velocity over the inlet surface shown in Fig. 4(2), and the wall temperature is set to a uniform 20 °C. The FLUENT (ANSYS, Inc.) software package is used for the fluid analysis [32]. In this analysis, approximately 3 million tetrahedral elements are used.

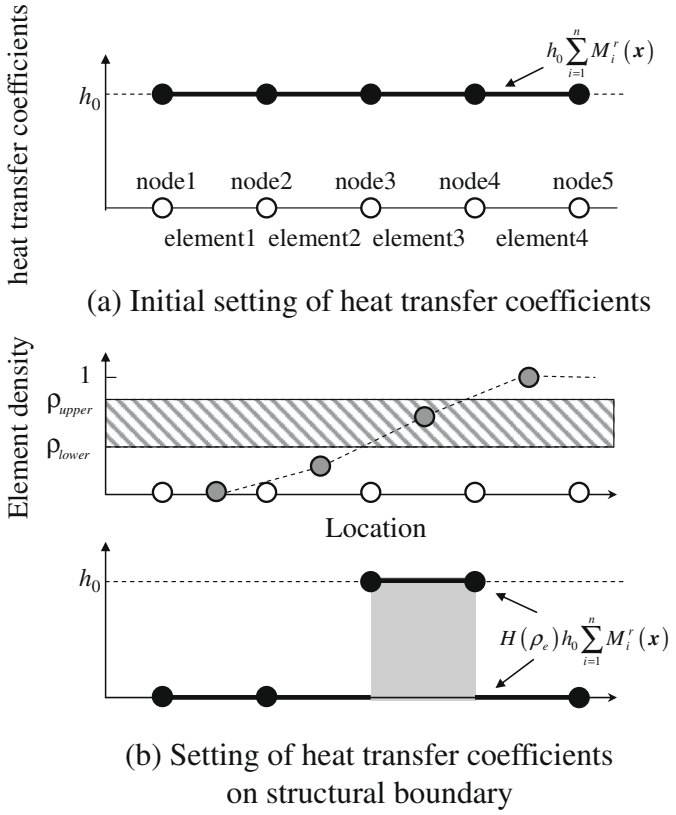

Fig. 3. Schematic view of setting method of heat transfer coefficients.

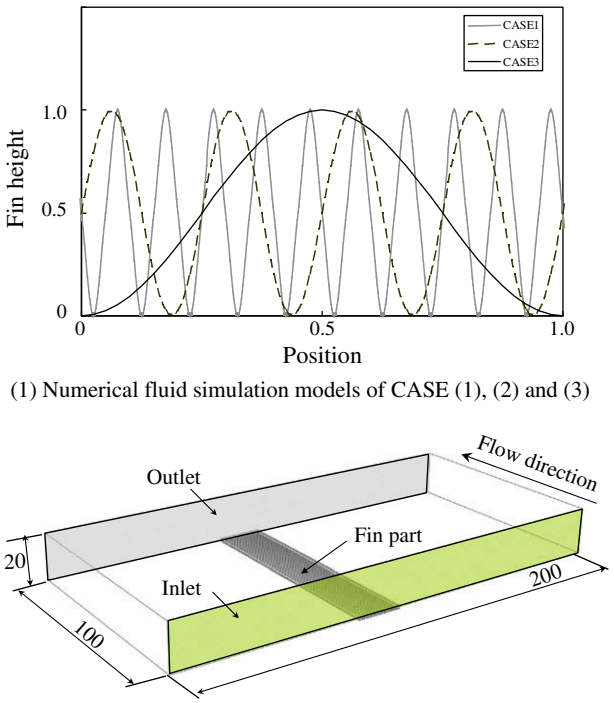

Fig. 4. Setting of numerical simulation model.

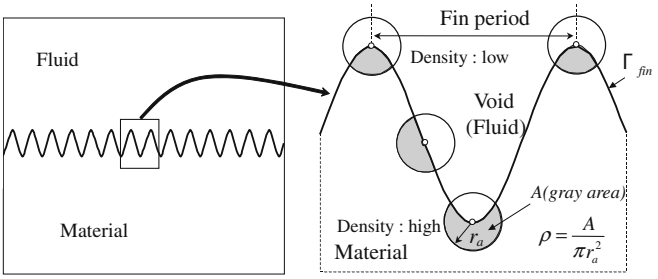

Fig. 5. Material density in a numerical fluid simulation model.

Next, we introduce parameters relating to the heat transfer coefficients. As shown in Fig. 5, circles with radius r_a and their centers located on the fin boundaries are set, defining the areas A that are the intersection of the circle and the fin profile, yielding a density ρ defined by Eq. (26) for each evaluation point. r_a is assumed to 0.05, which is determined as a half of the shortest fin period among the models shown in Fig. 4(1).

$$\rho = \frac{A}{\pi r_a^2} \tag{26}$$

Furthermore, the fin tips are regarded as being the points of lowest density on the fin boundaries. According to Eq. (26) and Fig. 4(1), fins with shorter periods will have lower density at the fin tips, so the fin tip density is used as the fin period P, and it is set as follows.

$$P = min\rho \quad \text{on} \quad \Gamma_{fin} \tag{27}$$

where Γ_{fin} indicate the fin boundaries.

Next, a surrogate model is constructed with respect to density ρ and a period P calculated according to Eqs. (26) and (27). In our research, this surrogate model is constructed using the Radial Basis Function (R.B.F) [33], where linear-splines are used as a basis function in the R.B.F. The heat transfer coefficients can then be expressed as,

$$h_0(\boldsymbol{z}) = \sum_{j=1}^{m} a_j g_j(\boldsymbol{z}) + a_{m+1} \tag{28}$$

where $\boldsymbol{z} = (\rho, P)^T$, $g_j(\boldsymbol{z}) \equiv g(||\boldsymbol{z} - \boldsymbol{z}_j||)$ and m indicate the position of sampling points, the basis function and the number of sampling points, respectively, and values of a_j $(j = 1, 2, \cdots, m+1)$ are determined by solving the following equations.

$$\sum_{j=1}^{m} a_j g_j(z_i) + a_{m+1} = h_i \quad (j = 1, 2, \cdots, m) \tag{29}$$

$$\sum_{j=1}^{m} a_j = 0 \tag{30}$$

where h_i indicates the value of the heat transfer coefficient at sampling point i.

Fig. 6 shows the surrogate model constructed using Eqs. (26)–(28). Heat transfer coefficients are normalized to 1 for the largest value and the fin period P is also normalized to 1. As shown in this figure, the highest heat transfer coefficient h_0 is observed at the lowest density point, which lies at the fin tips, and the heat transfer coefficient is correspondingly minimized at the bottom of fin where the density is highest. Heat transfer coefficient in areas of high density and short fin period increases slightly as the fin period decreases further, due to the extrapolation of sampling data in the Radial Basis Function.

Using this surrogate model, the basic heat transfer coefficient is rewritten as follows,

$$h(\boldsymbol{x}) \approx h^h(\boldsymbol{x}) = H(\rho_e)\boldsymbol{M}^r(\boldsymbol{x})\boldsymbol{h} = H(\rho_e)\sum_{i=1}^{n} M_i^r(\boldsymbol{x}) h_0(\rho_i, P) \tag{31}$$

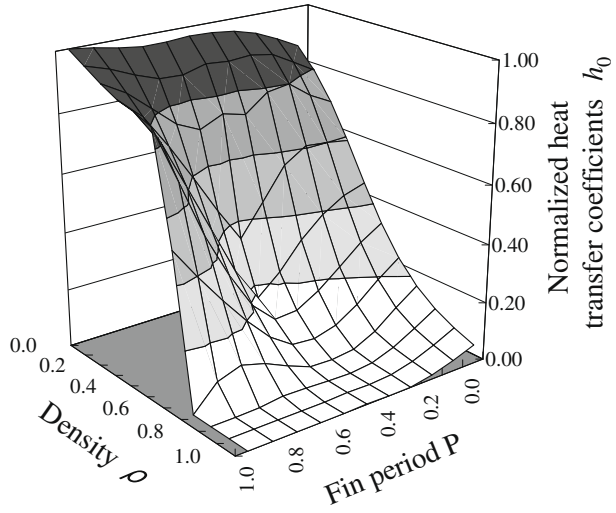

Fig. 6. Surrogate model with respect to normalized heat transfer coefficients using the Radial Basis Function.

where ρ_i and P respectively indicate the i-th node density and fin period, both of which are evaluated based on Eqs. (26) and (27), using the material densities obtained in the topology optimization.

2.6. Optimization algorithm

Fig. 7 shows a flowchart of the optimization. In the first step, the homogenized thermal conduction tensor $\boldsymbol{\kappa}^H$ is computed using the FEM. In the second step, the equilibrium (9) is solved using the FEM and nodal temperature vector $\boldsymbol{T}$ is obtained. In the third step, the objective function and volume constraint are calculated. The design variables R_i $(i = 1, 2, \cdots, n)$ are bounded according to Eq. (32) below, to avoid singularities in the FE analysis, although these design variables are theoretically bounded by Eq. (3).

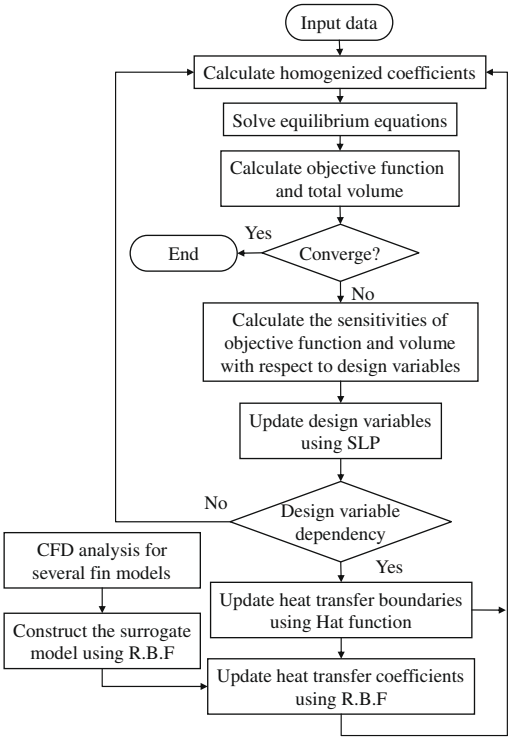

Fig. 7. Flow chart of optimization method.

$$0 \leqslant R_i \leqslant r_{upp} < 1 \tag{32}$$

where r_{upp} is the upper bound of the design variables, and is set to a sufficiently large number, but less than one. In the fourth step, the sensitivities of the objective function and volume with respect to design variables are computed if the objective function has not converged. In the fifth step, the design variables are updated using SLP. The advantage of using SLP is that almost all optimization problems can be solved rather quickly, without setting artificial parameters.

After updating the design variables using SLP, the design-dependent heat transfer coefficients are set according to Eq. (23) on the structural boundaries extracted by the smeared-out Hat function. In cases where heat transfer coefficient dependencies with respect to shape are taken into account, the coefficients are updated using Eq. (31), and the optimization procedure is then repeated from the first step.

2.7. Design sensitivity analysis

Let $\boldsymbol{K}$, $\boldsymbol{K}_h$, $\boldsymbol{q}$, $\boldsymbol{Q}$ and $\boldsymbol{H}$ respectively be the thermal conduction matrix, heat transfer matrix, heat flux vector, internal heat generation vector and heat transfer vector in the extended design domain D after FE discretization is carried out. Then, equilibrium equation (9) and the objective function F in Eq. (17) can be respectively rewritten as

$$(\boldsymbol{K}+\boldsymbol{K}_h)\boldsymbol{T} = \boldsymbol{q}+\boldsymbol{Q}+\boldsymbol{H} \tag{33}$$

$$F = \frac{1}{2}\boldsymbol{T}^T\boldsymbol{K}\boldsymbol{T} + \frac{1}{2}\boldsymbol{T}^T\boldsymbol{K}_h\boldsymbol{T} - \boldsymbol{T}^T(\boldsymbol{q}+\boldsymbol{Q}+\boldsymbol{H}) \tag{34}$$

The sensitivity of the objective function with respect to the i-th design variable R_i is obtained by

$$\begin{aligned}\frac{\partial F}{\partial R_i} = {} & \frac{1}{2}\left(\frac{\partial \boldsymbol{T}^T}{\partial R_i}\boldsymbol{K}\boldsymbol{T} + \boldsymbol{T}^T\frac{\partial \boldsymbol{K}}{\partial R_i}\boldsymbol{T} + \boldsymbol{T}^T\boldsymbol{K}\frac{\partial \boldsymbol{T}}{\partial R_i}\right) \\ & - \frac{1}{2}\left(\frac{\partial \boldsymbol{T}^T}{\partial R_i}\boldsymbol{K}_h\boldsymbol{T} + \boldsymbol{T}^T\frac{\partial \boldsymbol{K}_h}{\partial R_i}\boldsymbol{T} + \boldsymbol{T}^T\boldsymbol{K}_h\frac{\partial \boldsymbol{T}}{\partial R_i}\right) \\ & - \frac{1}{2}\frac{\partial \boldsymbol{T}^T}{\partial R_i}(\boldsymbol{q}+\boldsymbol{Q}+\boldsymbol{H}) - \boldsymbol{T}^T\frac{\partial(\boldsymbol{q}+\boldsymbol{Q}+\boldsymbol{H})}{\partial R_i}\end{aligned} \tag{35}$$

On the other hand, differentiating the equilibrium equation (9) with respect to R_i yields

$$\frac{\partial(\boldsymbol{K}+\boldsymbol{K}_h)}{\partial R_i}\boldsymbol{T} + (\boldsymbol{K}+\boldsymbol{K}_h)\frac{\partial \boldsymbol{T}}{\partial R_i} = \frac{\partial(\boldsymbol{q}+\boldsymbol{Q}+\boldsymbol{H})}{\partial R_i} \tag{36}$$

Since matrix $\boldsymbol{K}$ is symmetric, by substituting Eqs. (33) and (36) into Eq. (35) the sensitivity of objective function can be rewritten as

$$\frac{\partial F}{\partial R_i} = \frac{1}{2}\boldsymbol{T}^T\frac{\partial(\boldsymbol{K}+\boldsymbol{K}_h)}{\partial R_i}\boldsymbol{T} - \boldsymbol{T}^T\frac{\partial(\boldsymbol{q}+\boldsymbol{Q}+\boldsymbol{H})}{\partial R_i} \tag{37}$$

where the second term in the right-hand portion of Eq. (37) corresponds to a design-dependent effect.

3. Numerical examples

Numerical examples for the heat flux, internal heat generation, and heat convection loads for 2-dimensional problems are presented to confirm the utility of the proposed method. In all cases, the isotropic material has a thermal conductivity 50 W/mK and the initial configuration of the fixed design domain has a uniform microstructure distribution where R_i ($i = 1,\cdots,n$) is set to 0.9.

3.1. Effect of heat flux boundary conditions upon thermal conductor

Fig. 8 shows the design domain for example problem 1. As shown in this figure, the shape of the design domain is a 5 m × 5 m square, and a temperature $T = 0$ °C is imposed at boundaries Γ_T. Furthermore, a heat flux of 1 W/m^2 is also applied to boundary Γ_q. Here, we examine the relationship between the length of the boundaries shown in Fig. 8(a)–(d) and the optimal configurations. The upper limit of the volume constraint Ω_s is set to 30% of the entire design domain and the optimization is carried out using 50 × 50 elements.

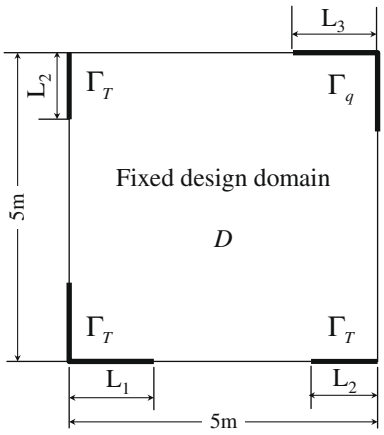

Fig. 8. Design domain for design problem 1. (a) $L_1 = 0.5$, $L_2 = 0.0$, $L_3 = 0.5$, (b) $L_1 = 1.5$, $L_2 = 1.0$, $L_3 = 0.5$, (c) $L_1 = 5.0$, $L_2 = 0.0$, $L_3 = 0.5$, (d) $L_1 = 5.0$, $L_2 = 0.0$, $L_3 = 5.0$.

Fig. 9 shows the optimal configurations. No checkerboards emerged in any of the figures, and clear, optimal configurations are obtained in every case. In Fig. 9(a), the heat flux is applied at the upper right corner, and the bottom corner of the left side is assumed to be at $T = 0$ °C. The optimal configuration then becomes a straight-line structure that extends from the upper right corner to lower left corner. In contrast, when Γ_T is expanded as shown in Fig. 9(b), the optimal configuration is expanded toward the newly specified temperature boundary, as shown in Fig. 9(b). Furthermore, if the temperature boundary is expanded to an entire side of the square design domain, as shown in Fig. 9(c), the optimal configuration becomes a curved shape, due, we assume, to the combined influence of the distant temperature boundary and the closer fixed temperature boundary. Fig. 9(d) shows the optimal configuration when the heat flux boundary Γ_q is expanded to the entire side of the square design domain. In this case, a shape deploys along the heat flux boundary and is influenced by the temperature boundary. From a physical point of view, it would be better if the branch in

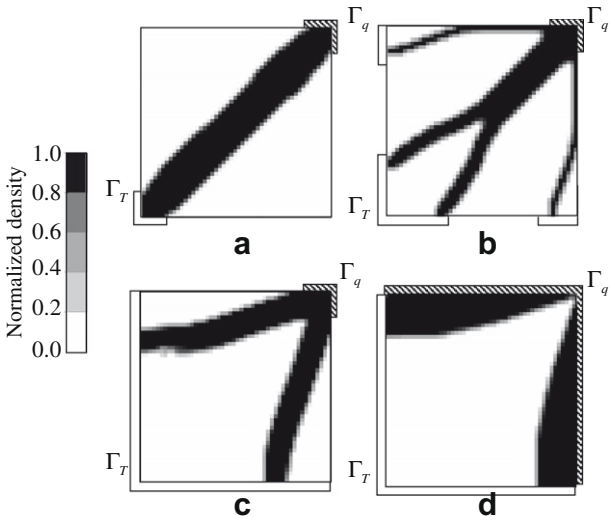

Fig. 9. Optimal configurations of design problem 1. (a) $L_1 = 0.5$, $L_2 = 0.0$, $L_3 = 0.5$, (b) $L_1 = 1.5$, $L_2 = 1.0$, $L_3 = 0.5$, (c) $L_1 = 5.0$, $L_2 = 0.0$, $L_3 = 0.5$, (d) $L_1 = 5.0$, $L_2 = 0.0$, $L_3 = 5.0$.

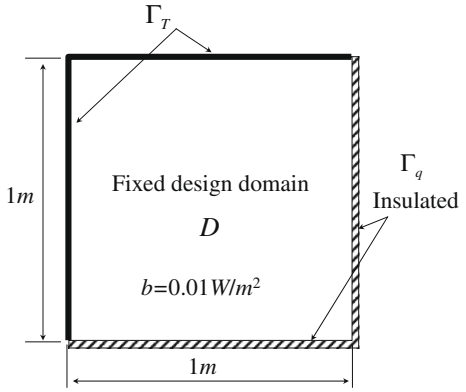

Fig. 10. Design domain for design problem 2.

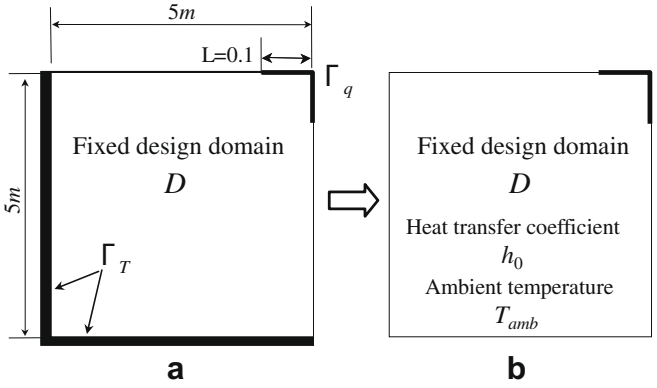

Fig. 12. Design domain for design problem 3. (a) boundary condition during the first N_T iteration, (b) boundary condition from $N_T + 1$ iteration.

the bottom right corner of the void region in Fig. 9(b) and (c) were as short and thick as possible for this problem. We conjecture that the discrepancy between this ideal and the numerical result is due to local optimality encountered by our optimization method.

3.2. Effect of design-dependent internal heat generation loads upon thermal conductor

Fig. 10 shows the design domain for example problem 2. As shown in this figure, the shape of the design domain is a 1 m × 1 m square, and a temperature $T = 0$ °C is imposed at boundary Γ_T. An insulator condition is also applied at boundary Γ_q, and an internal heat generation output of 0.01 W/m^2 is uniformly applied over the entire design domain. The upper limit of the volume constraint Ω_s is 40% of the entire design domain and the optimization is carried out using 200 × 200 elements. The optimization is performed with and without design variable dependencies for the internal heat generation, to examine the influence that design variable dependency has on the optimal configurations.

Fig. 11 shows a comparison of the optimal configurations in cases with and without design variable dependency, with respect to the internal heat generation. As shown in Fig. 11(a), in the case where we assume that the internal heat generation loads ignore design dependencies, small fin shapes emerge near the diagonal extending to boundary Γ_T in the fixed design domain, to diffuse the internal heat generation existing over the entire design domain. On the other hand, when design-dependent internal heat generation loads are taken into account, the material density as well as the internal heat generation values become small in the fixed design domain at locations far from boundary Γ_T, and the optimal configuration displays the relatively small fin shape shown in Fig. 11(b). These results show that design variable dependencies play a significant role in the optimal configuration results with respect to internal heat generation, and that our proposed method

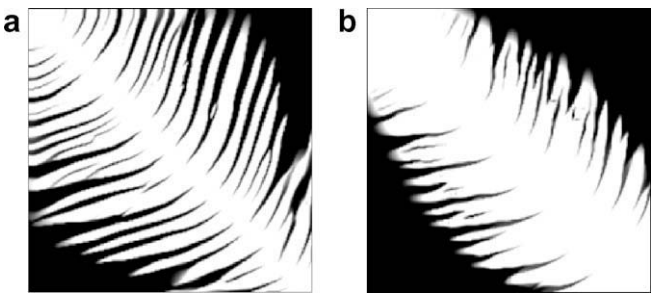

Fig. 11. Optimal configurations of design problem 2. (a) without dependency on design variables, (b) with dependency on design variables.

can yield optimal structural configurations which correlate well with the amount of actual internal heat generation.

3.3. Effect of design-dependent heat convection loads upon thermal conductor

Fig. 12 shows the design domain for example problem 3. The boundary Γ_T in the design domain, a 5 m × 5 m square, is imposed at $T = 0$ °C, and a heat flux of 1 W/m^2 is applied at boundary Γ_q. Heat convection loads consisting of heat transfer coefficients $h_0 = 0.1$ W/m^2 K and ambient temperatures $T_{amb} = 0$ °C, are set over the entire design domain as shown in Fig. 12(b). The upper limit of the volume constraint Ω_s is set to 30% of the entire design domain, ρ_{lower} and ρ_{upper} in the smeared-out Hat function are set to 0.3 and 0.9 respectively, and parameter ε in the smeared-out Heaviside function is set to 0.001, which is based on our numerical examination. The optimization is carried out using 200 × 200 elements.

In this example, until the maximum material density exceeds ρ_{lower} (we call this iteration number N_T, optimization proceeds using the boundary condition shown in Fig. 12(a), i.e., imposed temperature is in effect. From the next iteration, the temperature constraint on Γ_T is removed and Eq. (22) is applied to extract the design-dependent heat convection boundaries. In this example, shape dependencies with respect to heat transfer coefficients are not considered. Fig. 13(1) shows the history of the optimal configurations during the optimization. Checkerboards are absent, and many small fins are present, which diffuse heat in the thermal conductor. Fig. 13(2) and (3) show the history of temperature distribution and temperature at top right corner of the design domain, where the thermal conductor is subject to the highest temperature. As shown in these figures, the temperature in a configuration decreases as the optimization process is carried out.

Next, we examine the reason for removing the imposed temperature constraint at an intermediate stage of the optimization process. Fig. 14(1) shows the material distributions for cases where the imposed temperature constraint was removed after respective numbers of iterations had been carried out, (a) $N_T = 15$, (b) $N_T = 30$, (c) $N_T = 50$, (d) $N_T = 100$, respectively. The optimal configurations are shown in Fig. 14(2). In our proposed method, a non-uniform material distribution is required in order to extract structural boundaries. However, as shown in Fig. 14(2) (c) and (d), when an imposed temperature constraint is maintained until clear configurations emerge, the optimal configurations are strongly affected by the configuration when the temperature constraint is removed. Since elements whose material density is within $\rho_{lower} < \rho_e < \rho_{upper}$ are regarded as the set of the structural boundaries to be extracted by the Hat function, we remove the imposed temperature constraint after the iteration

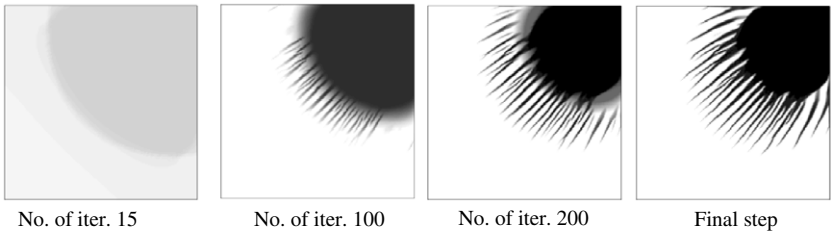

(1) Convergence history for design problem 3

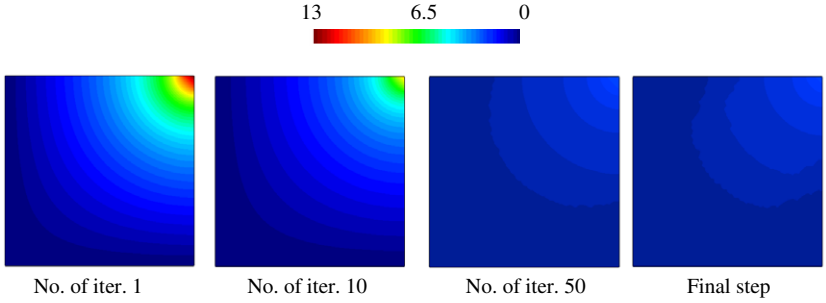

(2) History of temperature distribution for design problem 3

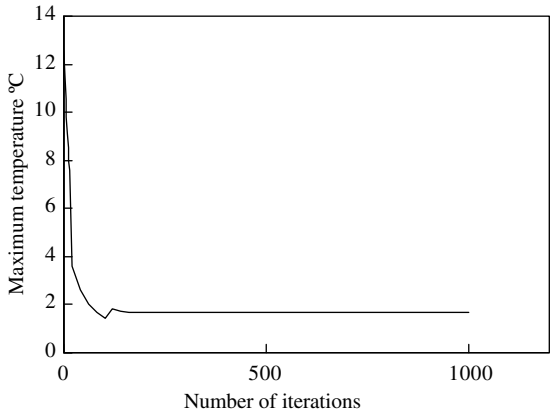

(3) History of temperature at right top point for design problem 3

Fig. 13. History of optimization for design problem 3.

where the updated material density value exceeds ρ_{lower}, which is set to 0.3 in our research.

Next, the influence that values of heat transfer coefficient and thermal conductivity have upon the optimal configurations is investigated. Fig. 15 shows the results of examples that use the following combinations of 3 heat transfer coefficients $h_0 = 0.01\ \mathrm{W/m^2\,K}$; $h_0 = 0.1\ \mathrm{W/m^2\,K}$; $h_0 = 1.0\ \mathrm{W/m^2\,K}$ and 2 thermal conductivities $\lambda = 5.0\ \mathrm{W/mK}$; $50\ \mathrm{W/mK}$. With thermal conductivity fixed, the optimal configurations show that lower heat transfer coefficients tend to increase the length of heat transfer boundary Γ_h and higher heat transfer coefficients tend to minimize the distance from the heat flux boundary Γ_q. Thus, when considering design-dependent heat convection loads, it is important to recognize that the optimal configurations are strongly influenced by the heat transfer coefficient values.

Here we explain why such optimal configurations are obtained, using a one-dimensional steady-state heat conduction model with heat convections. We assume that the heat flux through the structure is Q and that the heat transfer coefficient and ambient temperature for the high and low temperature fluid sides are respectively h_1, t_{f1}, and h_2, t_{f2}, and that the heat transfer area is S. The heat flux through the structure is then given as

$$Q = K(t_{f1} - t_{f2})S \tag{38}$$

where K indicates the coefficient of heat transmission shown below.

$$K = \frac{1}{(1/h_1) + (l/\lambda) + (1/h_2)} \tag{39}$$

where l and λ indicate the thickness of the structure and its thermal conductivity, respectively. Eq. (38) shows that larger values of S and K are necessary if the amount of heat transfer through the structure is to be increased. In Eq. (39), K depends on l, λ and h, therefore the length of the optimal configuration that can maximize temperature diffusivity depends on the value of the heat transfer coefficients when the material is selected. Increasing the heat transfer area is an effective means for increasing the release of heat, so a profuse array of fins emerges in the fixed design domain to minimize temperature, as shown in Fig. 15. If, however, a higher heat transfer coefficient value is set, the optimal configuration has a much larger number of much shorter fins, to increase the heat transfer area while minimizing the distance from the corner heat source. This minimizes the contribution of l/λ to K.

The value of K depends on the relation between the heat transfer coefficients and the thermal conductivity. Therefore, the same optimal configurations are obtained as shown in Fig. 15, as long as the ratio of the heat transfer coefficient to

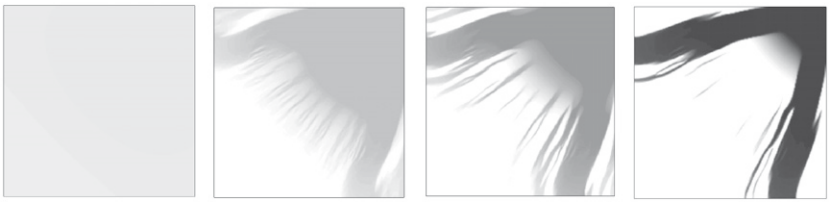

(1) Density distributions when imposed temperature boundary conditions are removed. (a) N_T =15, (b) N_T =30, (c) N_T =50, (d) N_T =100

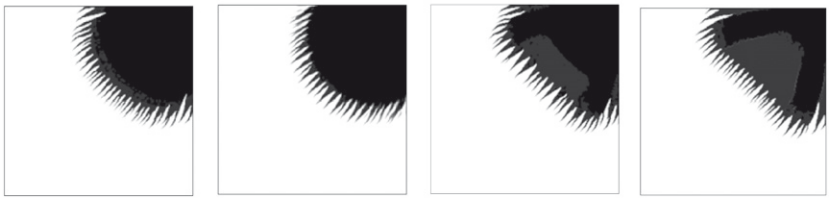

(2) Optimal configurations corresponding to the iteration number when the imposed temperature boundary condition is removed. (a) N_T =15, (b) N_T =30, (c) N_T =50, (d) N_T =100

Fig. 14. Relationship between optimal configurations and number of iteration when the imposed temperature boundary condition is removed.

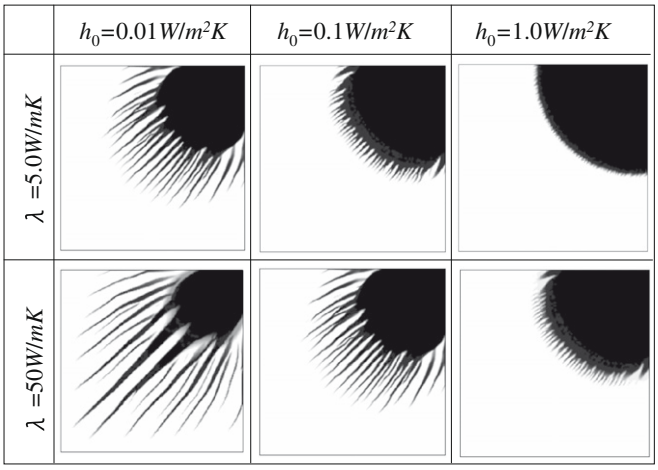

Fig. 15. Relationship between thermal conductivity and heat transfer coefficient shown in optimal configurations.

the thermal conductivity is preserved. The validity of our proposed method is confirmed, since identical results are obtained for a given ratio of heat transfer coefficient to thermal conductivity.

3.4. Heat pipe design problem using topology optimization

The next example is a pipe design problem. Fig. 16 shows the design domain for design problem 4, which is a 5 m × 5 m square with an imposed temperature T = 0 °C at P_T, a heat flux of 1 W/m^2 applied to boundary Γ_q and the other sides insulated. Heat convection loads which consist of heat transfer coefficients h_0 and ambient temperature T_{amb}, are set on all nodes of the design domain. The upper limit of the volume constraint Ω_s is set to 30% of the entire design domain. Computations are carried out using a single quadrant of the model, as shown in Fig. 16, to save calculation time, and the optimization is carried out using 200 × 200 elements.

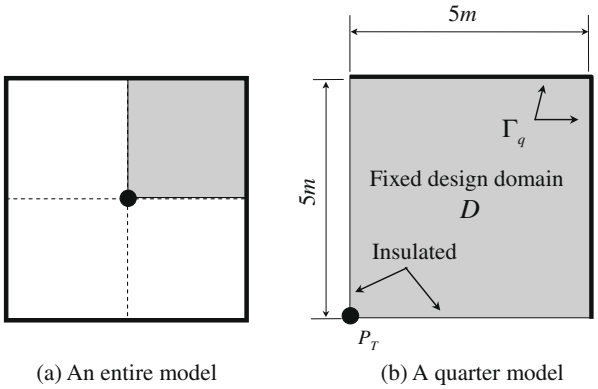

Fig. 16. Design domain for design problem 4.

Fig. 17 shows the optimal configurations. Material is distributed along the four edges that are the heat convection boundaries. The thinner structures more effectively dissipate heat, but when heat transfer coefficient values are comparatively low, corresponding to lower fluid velocities, many small fins are generated, expanding the effective area for heat transfer.

Here we interpret the optimal configurations using Eq. (40), which denotes the Biot number. If we set a lower heat transfer

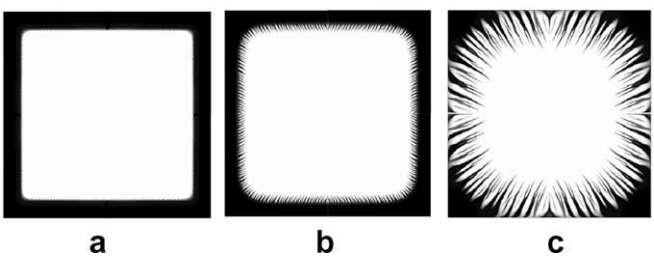

Fig. 17. Optimal configurations of design problem 4. (a) h_0 = 10.0 W/m^2 K, T_{amb} = 0 °C, (b) h_0 = 1.0 W/m^2 K, T_{amb} = 0 °C, (c) h_0 = 0.1 W/m^2 K, T_{amb} = 0 °C.

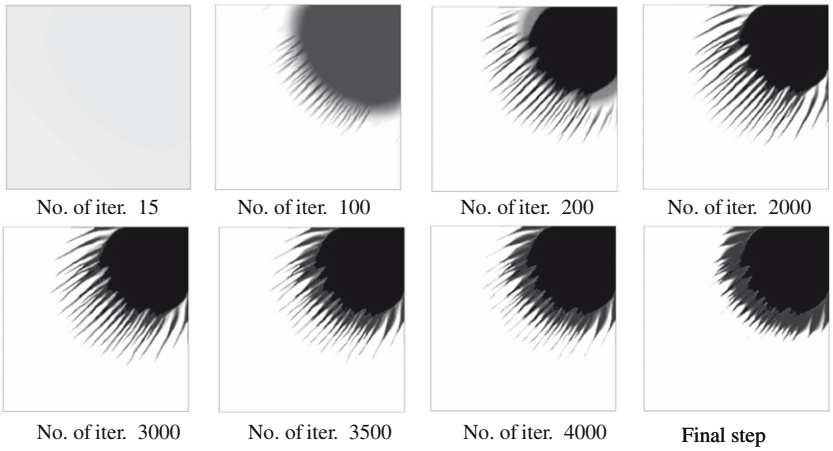

Fig. 18. History of optimization of design problem 3, considering shape dependencies with respect to heat transfer coefficients.

coefficient which corresponds to a smaller Biot number, then a larger value of l is required to increase the amount of heat transferred from the surface, because the heat transfer coefficient is already set as the boundary condition, with the result that many small fins are generated to expand the heat transfer boundary, as shown in Fig. 17(c). On the other hand, if we set a higher heat transfer coefficient, a smaller value of l, equivalent to a higher thermal conductivity setting in Eq. (40), is required to improve the release of heat in a structure such as shown in Fig. 17(a).

$$Bi = \frac{hl}{\lambda_{material}} \tag{40}$$

3.5. Optimal configuration considering shape-dependent heat transfer coefficients

In this example, we consider shape dependencies with respect to the heat transfer coefficients. Optimization is started from the final step of design problem 3 in Fig. 13(1). From the next step, the shape dependencies with respect to the heat transfer coefficients are considered, based on Eq. (31).

Fig. 18 shows the optimization history and optimal configurations considering shape-dependent heat transfer coefficients. As shown in Fig. 18, in high-density areas at the fin bases, the values of the heat transfer coefficients are low, and voids in the near neighborhood are replaced with material as the optimization procedure is iterated. On the other hand, in low-density areas at the tips of the fins, heat transfer coefficient values become high, and thermal conductivity can be exploited to improve the diffusion of heat. The result, as seen in the optimal configuration, is that a large number of short fins maximizes the heat transfer area and minimizes the distance from the heat source. The optimal configuration obtained shown in Fig. 18 differs dramatically from the result shown in Fig. 13(1), where shape dependencies with respect to heat transfer coefficients were ignored. Thus, for temperature diffusion optimization problems that include heat transfer boundary conditions, consideration of shape dependencies with respect to heat transfer coefficients is indispensable.

4. Conclusions

In this paper, we developed a structural optimization method for the design of thermal conductors that aim to maximize temperature diffusivity. We obtained the following results.

(1) The homogenization design method was extended to thermal problems, in which continuous material distribution is assumed using C^0-continuous interpolation functions in the fixed design domain.
(2) The maximization problem to maximize temperature diffusivity was formulated using an objective function of total potential energy that can be treated as maximization problems for both Neumann and Dirichlet type boundary conditions.
(3) Design-dependent internal heat generation loads were formulated as a function of design variables, and also design-dependent heat convection loads were formulated using material density in elements and a Hat function, to extract the boundaries of the structure being optimized so that heat transfer boundary conditions can be set.
(4) A new method was developed for dealing with shape-dependencies with respect to heat transfer coefficients in the topology optimization scheme, using a surrogate model.
(5) An optimization problem was constructed based on the optimization formulation, incorporating the above objective function and sequential linear programming (SLP).
(6) Several numerical examples were provided to examine the characteristics of the optimal configurations for typical thermal boundary conditions. It was confirmed that the proposed method provides checkerboard-free optimal configurations in all examples. It was also confirmed that design-dependent and shape-dependent effects upon internal heat generation and heat convection loads play significant roles in the design of thermal conductors, and that the proposed method can obtain solutions that successfully exploit actual heat transfer and conduction phenomenon.

References

[1] M.P. Bendsøe, N. Kikuchi, Generating optimal topologies in structural design using a homogenization method, Comput. Meth. Appl. Mech. Eng. 71 (1988) 197–224.
[2] K. Suzuki, N. Kikuchi, A homogenization method for shape and topology optimization, Comput. Meth. Appl. Mech. Eng. 93 (1991) 291–318.
[3] A.R. Diaz, N. Kikuchi, Solutions to shape and topology eigenvalue optimization problems using a homogenization method, Int. J. Num. Meth. Eng. 35 (1992) 1487–1502.
[4] A. Cherkaev, Variational Method for Structural Optimization, Springer-Verlag, 2000. 117–141.
[5] G. Allaire, Shape optimization by the homogenization method, Springer-Verlag, 2002. 189–257.
[6] J. Haslinger, A. Hillebrand, T. Kärkkäinen, M. Miettinen, Optimization of conducting structures by using the homogenization method, Struct. Multidiscip. Optimiz. 24 (2002) 125–140.

[7] A. Iga, S. Nishiwaki, K. Izui, M. Yoshimura, Topology optimization for thermal problems based on assumed continuous approximation of material distribution, Trans. Jpn. Soc. Mech. Eng. C 73 (2007) 2426–2433.
[8] M.P. Bendsøe, Optimal shape design as a material distribution problem, Struct. Optimiz. 1 (1989) 193–202.
[9] C. Seonho, Y.C. Jae, Efficient topology optimization of thermo-elasticity problems using coupled field adjoint sensitivity analysis method, Finite Elements Anal. Design 41 (2005) 1481–1495.
[10] Q. Li, G.P. Steven, O.M. Querin, Y.M. Xie, Shape and topology design for heat conduction by evolutionary structural optimization, Int. J. Heat Mass Trans. 42 (1999) 3361–3371.
[11] L. Yin, G.K. Ananthasuresh, A novel topology design scheme for the multi-physics problems of electro-thermally actuated compliant micromechanism, Sensors Actuators A 97–98 (2002) 599–609.
[12] Y.M. Xie, G.P. Steven, Evolutionary Structural Optimization, Springer-Verlag, 1997.
[13] A. Gersborg-Hansen, M.P. Bendsøe, O. Sigmund, Topology optimization of heat conduction problems using finite volume method, Struct. Multidiscip. Optimiz. 31 (2006) 251–259.
[14] Y. Li, K. Saito, N. Kikuchi, Topology optimization of thermally actuated compliant mechanisms considering time-transient effect, Finite Elements Anal. Design 40 (2004) 1311–1317.
[15] O. Sigmund, Design of multiphysics actuators using topology optimization Part1: One metal structures, Comput. Meth. Appl. Mech. Eng. 190 (2001) 6577–6604.
[16] C.G. Zhuang, Z.H. Xiong, H. Ding, A level set method for topology optimization of heat conduction problem under multiple load cases, Comput. Meth. Appl. Mech. Eng. 196 (2007) 1074–1084.
[17] B.C. Chen, N. Kikuchi, Topology optimization with design-dependent loads, Finite Elements Anal. Design 37 (2001) 57–70. 2001.
[18] B. Bourdin, A. Chamblle, Design-dependent loads in topology optimization, Control Optimiz. Calc. Var. 9 (2003) 19–48.
[19] T. Gao, W. Zhang, J. Zhu, Y. Xu, Topology optimization of heat conduction problem involving design-dependent effect, in: Proceedings of the Forth China-Japan-Korea Joint Symposium on Structural and Mechanical Systems, Kunming, China, November 6–9, 2006.
[20] G.H. Yoon, Y.Y. Kim, The element connectivity parameterization formulation for the topology design optimization of multiphysics system, Int. J. Num. Meth. Eng. 64 (2005) 1649–1677.
[21] J.C. Ryu, Y.Y. Kim, Density-dependent shape function approach for trouble-free topology optimization for heat transfer problems including side convection, in: Proceedings of 7th World Congress on Structural and Multidisciplinary Optimization, Seoul, Korea, May 21–25, 2007.
[22] T.E. Bruns, Topology optimization of convection-dominated, steady-state heat transfer problems, Int. J. Heat Mass Transfer 50 (2007) 2859–2873.
[23] D. Fujii, N. Kikuchi, Improvement of numerical instabilities in topology optimization using SLP method, Struct. Optimiz. 19 (2000) 113–121.
[24] B. Blaise, Filters in topology optimization, Int. J. Num. Meth. Eng. 50 (2001) 2143–2158.
[25] R.B. Haber, C.S. Jog, M.P. Bendsøe, A new approach to variable-topology shape design using a constraint on parameter, Struct. Optimiz. 11 (1996) 1–12.
[26] K. Matsui, K. Terada, Continuous approximation of material distribution for topology optimization, Int. J. Num. Meth. Eng. 59 (2004) 1925–1944.
[27] S. Rahmatalla, C.C. Swan, A Q4/Q4 continuum structural topology optimization implementation, Continuous approximation of material distribution for topology optimization, Struct. Multidisciplinary Optimiz. 27 (2004) 130–135.
[28] J.G. Michel, H. Moulinec, P. Squet, Asymptotic Analysis for Periodic Structures, North-Holland, Amsterdam, 1978.
[29] K. Terada, N. Kikuchi, A class of general algorithms for multi-scale analyses of heterogeneous media, Comput. Meth. Appl. Mech. Eng. 190 (2001) 5427–5464.
[30] H. Azegami, C.Z. Wu, Domain optimization analysis in linear elastic problems: approach using traction method, JSME Int. J. A 39 (1996) 272–278.
[31] E.W. Dittus, L.M.K. Boelter, Heat transfer in 80 automobile radiators of the tubular type, Univ. Calif. Publ. Eng. 2–3 (1930) 443–461.
[32] ANSYS, Inc., FLUENT 6.3 Documentation, 2007.
[33] E.F. Gregorv, Meshfree approximation methods with MATLAB, World Science, 2007. 53–61.